Voltage and current distribution in a doubly connected two-dimensional quantum Hall system

M. Oswald and J. Oswald
University of Leoben, Institute of Physics, Franz Josef Street 18, A-8700 Leoben, Austria

R. G. Mani
Harvard University, Gordon McKay Laboratory of Applied Science, 9 Oxford Street, Cambridge, Massachusetts 02138, USA
(Received 18 January 2005; published 15 July 2005)

Numerical simulations are compared with experimental results for the so-called "anti-Hall bar within a Hall bar" configuration, which is a doubly connected, double-boundary electronic system that has been experimentally investigated by Mani. Here, we illustrate the application of a network model for magnetotransport, which allows the evaluation of the longitudinal and Hall voltages, and the current distribution, in this geometry. Thus, we rebuild the experimental configuration, including the sample geometry with the boundary conditions, and the two independent floating current sources, within our network. As in the reported experiment, we realize the Hall voltages and longitudinal voltages at both the inner and outer boundaries. In excellent agreement with Mani's experiments, we find that the Hall voltages at the inner (anti-Hall bar) and outer (Hall bar) boundaries depend just on the individual current injected via the corresponding boundary, while the longitudinal voltage depends exactly on the sum of the injected currents.

DOI: 10.1103/PhysRevB.72.035334 PACS number(s): 73.43.Cd, 73.43.Fj, 73.43.Qt, 73.43.Jn

I. INTRODUCTION

The quantized Hall effect (QHE) stimulated a broad experimental and theoretical study of the two-dimensional electron system that was aimed at understanding the physical origin of this remarkable phenomenon.[1] Laughlin[2] provided an explanation of the observed Hall quantization by carrying out a gedanken gauge argument experiment on a two-dimensional electron system, which was rolled up into a cylinder. The resulting theory implied a bulk origin for the QHE after presuming a persistent bulk current and insensitivity to basic features such as the sample topology, the existence of current contacts, and the connectivity of current and voltage contacts via a boundary. Büttiker[3] presented a supplementary perspective, utilizing a Landauer formalism, that emphasized the special role in the quantized Hall effect for the quantized conductance associated with edge currents (EC's).[4,5] After more than two decades of study, these theoretical perspectives constitute the most widely used approaches for understanding the QHE that is observed in experiment.

In order to determine the relative contributions of the bulk and edge current, Mani developed an experimental configuration that combined aspects of the Hall geometry, which is often investigated in the laboratory, with the doubly connected topology of Laughlin's cylinder.[6–8] Mani's resulting inversion-symmetric "anti-Hall bar within a Hall bar" configuration (see Fig. 1) included a planar doubly connected specimen with current and voltage contacts on both the interior and exterior boundaries, and a current source attached to each boundary. Thus, Mani performed measurements using two independent floating current sources, one for the exterior boundary Hall bar and the other for the interior boundary anti-Hall bar. The experiments showed dual simultaneous, independent Hall voltages, one at both the inner (anti-Hall bar) and outer boundaries (Hall bar) of the specimen. That is, the experiment demonstrated two simultaneous Hall effects, each with its own quantized Hall plateaus, in a single specimen.[6–8]

The same series of measurements indicated, however, that the longitudinal voltages were proportional to the sum of the currents injected via the two boundaries, and these voltages were identical at the Hall bar and anti-Hall bar. The results identified that the quantized Hall resistance measurement is the Hall effect measurement, which involves current and voltage contacts located on one and the same boundary.[6–8]

Here, we apply a network model to reproduce the experimental situation and examine the microscopics behind the realization of multiple simultaneous ordinary and quantized Hall effects in a single specimen. A supplementary aim is to provide further insight into the nature of the current distribution and the Hall effect measurement in the multiply connected specimen.

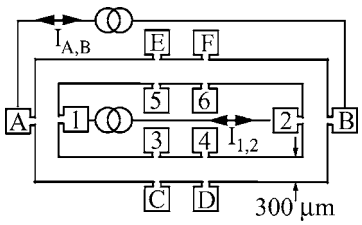

FIG. 1. The anti-Hall bar within a Hall bar experimental configuration utilized by Mani (Refs. 6–8). Here, the exterior boundary, associated contacts, and current source $I_{A,B}$ constitute the Hall bar, while the interior boundary, interior contacts, and the current supply $I_{1,2}$ make up the anti-Hall bar configuration. In the typical experiment, each of the floating current sources are set to a constant value, and the voltages on the Hall bar and/or anti-Hall bar are probed as a function of the ramped transverse magnetic field.

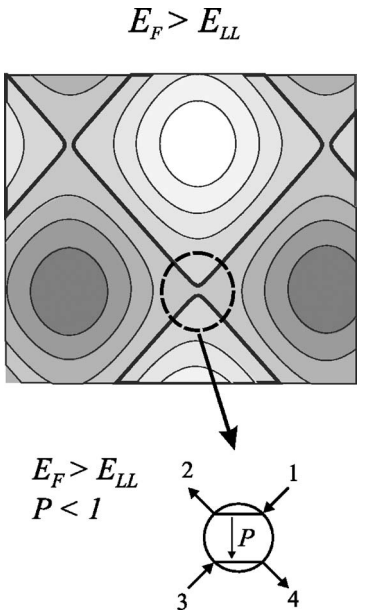

FIG. 2. Top: a contour plot of the lateral potential modulation, where the dark areas represent the valleys, and the light shaded areas represent the potential hills. In the figure, it is assumed that the hills are encircled clockwise, while the valleys are encircled counterclockwise. Bottom: at the saddle point, adjacent loops get close to each other, and this encounter is represented at the nodes of the network, by edge channel pairs. Here, $P<1$ corresponds to E_F above the LL center ($E_F>E_{LL}$). As shown by Eqs. (1), the output potentials μ_2 and μ_4 are completely determined by the input potentials μ_1 and μ_3. The EC pairs result from the loops of magnetic bound states encircling potential hills. If $E_F<E_{LL}$, the loops encircle potential valleys and the situation gets turned by 90°. However, this can be described by the same P, but setting $P>1$.

II. NETWORK MODEL

In this section, we provide a brief introduction to our network model. For more details, see Refs. 9–12. A common way to treat two-dimensional (2D) systems with disorder in the high-magnetic-field regime is to consider a lateral random potential modulation, which varies slowly on the scale of the magnetic length. This leads to magnetic bound states, which are extended along equipotential lines. For an infinite sample, all states are localized except for a particular energy, which corresponds to the center of the Landau level (LL). All states outside the center of the LL participate in transport only via quantum tunneling, which preferably happens at saddles of the potential landscape (see upper part of Fig. 2). The tunneling probability increases if the Fermi energy approaches the energy of the saddle points. The saddles can be considered as the nodes of a network with two incoming and two outgoing channels for each node. Since these channels result from magnetic bound states, they are physically equivalent to EC's. Although the basic idea of our network follows the Chalker-Coddington (CC) network model,[13] our handling of the nodes is substantially different: In contrast to a CC network our network does not use a transfer matrix for amplitudes and phases. We use transmission by tunneling and the key point in our model is that this tunneling is handled as a backscattering process in the EC picture. On this basis, we introduced a backscattering function P, which is formally equivalent to the ratio R/T of the Landauer-Büttiker formalism, with R and T being the reflection and transmission coefficient respectively (see lower part of Fig. 2). As mentioned before, the coupling depends on the position of the Fermi level and, hence, on the filling factor ν, which finally means that $P=P(\nu)$. The potential of the outgoing channels is completely determined by the potential of the incoming channels as follows:[9]

$$\mu_2 = \frac{\mu_1 + P\mu_3}{1+P}, \tag{1a}$$

$$\mu_4 = \frac{\mu_3 + P\mu_1}{1+P}. \tag{1b}$$

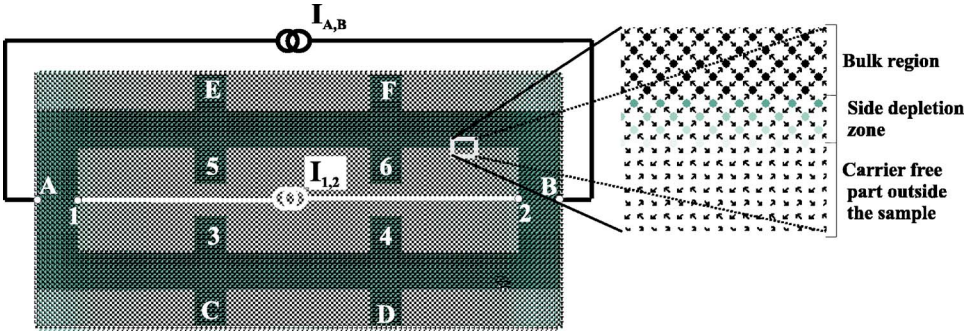

FIG. 3. (Color online) Sample layout for the network model of the anti-Hall bar within a Hall bar geometry with two independent current sources $I_{A,B}$ and $I_{1,2}$. The network consists of interconnected nodes with each of them representing a saddle point as shown in Fig. 2. These saddle points appear as shaded circles, with the gray scale applied towards indicating the local carrier density. The arrows, which are only visible in the expanded portion of the figure, represent the incoming and outgoing channels. The area with dark nodes indicates a constant carrier concentration of $n_0=4\times10^{11}$ cm^{-2}, which defines the bulk region of the sample. The gradual transition from dark gray to light gray represents the side depletion zone, from the bulk to zero carrier density at the sample boundaries (see the expanded portion of the figure). The current contacts are indicated by white dots at the inner and outer boundary of the sample. The Hall voltages are measured between the voltage probes (3) and (5) for the anti-Hall bar and between (C) and (E) for the Hall bar. The corresponding longitudinal voltages are measured between the voltage probes (3) and (4) for the anti-Hall bar and (C) and (D) for the Hall bar.

The whole network consists of a matrixlike arrangement of nodes, which are interconnected as shown in Fig. 3. The shape of the sample is defined by the lateral distribution of the carrier density on the network. The lateral carrier density profile itself is calculated from the distribution of lateral electrostatic bare potential, which is used as a tool for designing the shape of the sample. A zero bare potential indicates regions where the bulk carrier concentration is achieved and a nonzero positive potential is used to define gated regions of reduced carrier density and side depletion zones at the sample edges. If the potential is set sufficiently high, one obtains carrier free regions as needed for parts which should be "etched away" from the "wafer" in order to get the designed shape. In this way, each node of the network obtains its individual local carrier density and hence its own filling factor. As a consequence, each node obtains its corresponding individual coupling function $P_j(\nu(x,y))$, where x,y represent the location of the node in the x-y plane and j denotes the Landau level index. At this point it should also be mentioned that each involved LL is represented by a complete network and all these networks contribute in parallel. In Refs. 10 and 11, it has been shown that for each involved LL $P(\nu)=\exp(\Delta\nu/k)$ with $\Delta\nu$ being the filling factor relative to half filling ($\Delta\nu=\nu-0.5$) and k being a parameter, which accounts for the sharpness of the plateau to plateau transitions. Metallic contacts are defined within the network by interconnecting all channels of the different layers of the network (which are associated with the different LL's) at the designated location of the contact. In particular, current contacts are realized by setting them to a constant nonzero potential.

The actual calculation consists of two main parts: (I) For calculating the occupation numbers, standard procedures are used and the Fermi level in the bulk region is calculated by filling up the density of states (DOS) with the constant bulk carrier density. The DOS is composed by the superposition of the magnetic-field-dependent Gaussian-shaped DOS of spin split LL's. The Fermi level for regions of nonzero electrostatic bare potential like at the edges is forced to match the obtained (magnetic field dependent) Fermi level in the bulk. This allows for a self-consistent electrostatic potential and a rearrangement of the carrier density at the edges as first proposed by Chklovskii *et al.*[14] (II) The lateral carrier density profile obtained as above enters the nodes of the network and, in another self-consistent iteration procedure, the lateral distribution of the excitation voltage, which is introduced via the current contacts, is calculated. From this step, the potential difference for any designated pair of voltage probes is obtained as a function of the magnetic field. The current at the current contacts is calculated only after arriving at the self-consistent solution in the network, which allows one finally to calculate the various resistances. This means that, in principle, a constant supply voltage is used in the network model, instead of a constant supply current. Note, however, that this makes no difference for calculating the resistances of a standard QHE setup with a single current source. For achieving a constant-current mode, which is needed for the anti-Hall bar within a Hall bar configuration, the potentials at the current contacts are additionally varied in a proper way during the iteration procedure in order to get the required preset current. In this way, the constant current mode is realized, and it is possible to simulate also the simultaneous presence of several independent current sources such as that which appears in the anti-Hall bar within the Hall bar setup.

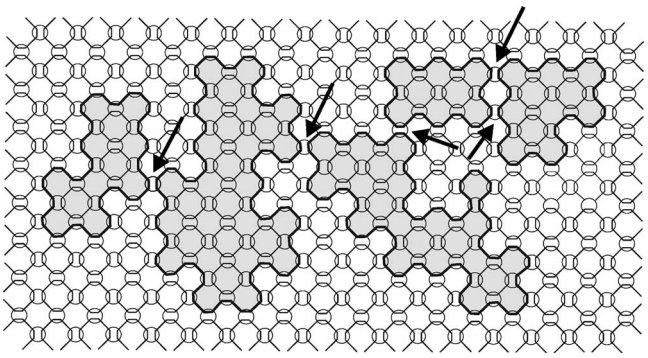

FIG. 4. Cutout of the bulk region showing the scheme of discretization of a random potential on the basis of our network model. The average filling factor of the associated Landau level is assumed to be close to $\nu=0.5$. The shaded regions represent $\nu>0.5$, which corresponds to a value of the coupling function $P\ll 1$, and the nonshaded regions represent $\nu<0.5$, which corresponds to $P\gg 1$. The basic grid consists of alternating rows and lines of nodes in same orientation. Therefore, a change from $P\ll 1$ to $P\gg 1$ appears graphically as a rotation of the nodes by 90° within a line and a row and, as can be seen in the figure, the corresponding nodes inside and outside the shaded area appear rotated against each other. Following now the interconnections in the network, one can see that in this way a channel at the boundary between $\nu>0.5$ and $\nu<0.5$ is automatically guided to follow these boundaries (bold line). In real samples, this corresponds to a arbitrarily shaped magnetic bound state following the contour lines of the random potential. Most of the nodes with $P\ll 1$ or $P\gg 1$ serve as some sort of switching device in the network and are therefore not physically active. Only those near the saddle of the real potential, where also the real magnetic bound states get close together (marked by the arrows), act physically as tunneling junctions within the framework of the Landauer-Büttiker formalism.

One more aspect should be addressed prior to the discussion of our results. At first glance, our regular network appears as a model of a periodic potential modulation, while the native random potential of a real sample suggests that a random network should be used instead. However, as will be demonstrated in the following, our network model can be understood also as a concept for effective discretization of a random network. Obviously, lateral long-range potential fluctuations will lead to a corresponding lateral fluctuation of the local filling factor, which, in turn, will lead to a lateral variation of the coupling function P of the nodes in our network. Suppose we wish to model a random potential on the basis of our regular network; then, we need to choose the grid period to be much less than the typical length scale of the potential fluctuations. This is qualitatively shown in Fig. 4: The system is supposed to be close to half filling, which means the possibility of bulk current flow. However, half filling means $\bar{\nu}=0.5$ on average and, due to the potential fluctuations, there will exist regions with locally $\nu>0.5$ and regions with locally $\nu<0.5$. In Fig. 4 the shaded regions represent $\nu>0.5$ and the nonshaded regions $\nu<0.5$. Most effective coupling at the nodes appears at $P=1$, which cor-

responds to exact half filling $\nu=0.5$. Due to the randomization of the potential, only few of all nodes will remain close to half filling and most of them will depart from half filling, which leads to a coupling function of $P \ll 1$ in the shaded regions and $P \gg 1$ outside. However, $P \ll 1$ or $P \gg 1$ means mainly that an incoming channel is almost completely transmitted either to the one or the other outgoing channel of the node, which appears as a rotation of a node by 90° upon changing from one case to the other. As can be seen in Fig. 4 in this way our network guides the transmitted channels all around the boundaries between $\nu > 0.5$ and $\nu < 0.5$. Therefore, in this case, most of the nodes are physically inactive, but just switching the whole transmitted channel to either the one or the other outgoing channel. Only the nodes near the saddles of the real potential, where $\nu \approx 0.5$ and where also the real loops of the magnetic bound states get close to each other, become physically active by coupling different real loops. On this basis our network can also be understood as an effective theoretical concept for setting up a random network with a discretization on a regular grid. However, already from considering Fig. 4, it is clear that a sufficient randomization of all conductor elements of a realistically shaped macroscopic sample geometry will require an increase in the size of the network by at least an order of magnitude in both directions in comparison to the simulations without randomization. For this reason, at the present, a "random network" modeling of the intricate anti-Hall bar within a Hall bar geometry is beyond our computing hardware capability. We tested instead the effect of randomization for a simple Hall bar geometry and found that the qualitative transport behavior and all observed trends remain the same. Only a certain amount of additional broadening appeared on the plateau transitions and the R_{xx} peaks. Indeed, only details of the curvature, especially in the tails of the R_{xx} peaks, appear sensitive to the details of the random potential. This is not surprising, however, since in a random potential, bulk current can be expected to become highly inhomogeneous near the percolation threshold. As we have aimed only to reproduce the main trends observed in magnetotransport studies of the anti-Hall bar within a Hall bar geometry in this paper, we performed our calculations without randomization, and expect the main conclusions drawn from the simulations to hold their validity.

III. RESULTS

The network used here for the simulation of the anti-Hall bar within a Hall bar structure is rectangular in shape and consists of 217×105 nodes. The width of the annulus (see device in Fig. 3) contains 16 nodes. The voltage probes, which are labeled from C–F for the Hall bar and 3–6 for the anti-Hall bar, are 16 nodes long and 14 nodes wide (see Fig. 3). Two independent constant current sources $I_{A,B}$ and $I_{1,2}$ are connected to the inner and outer boundaries of the sample as indicated in Fig. 3. The gradual change from dark to light gray at the boundaries indicates the side depletion zones, and this region is three nodes wide. The light-gray areas indicate vanishing carrier density, while the dark-gray area indicates the bulk region with a carrier density of $n_0=4\times10^{11}$ cm^{-2}.

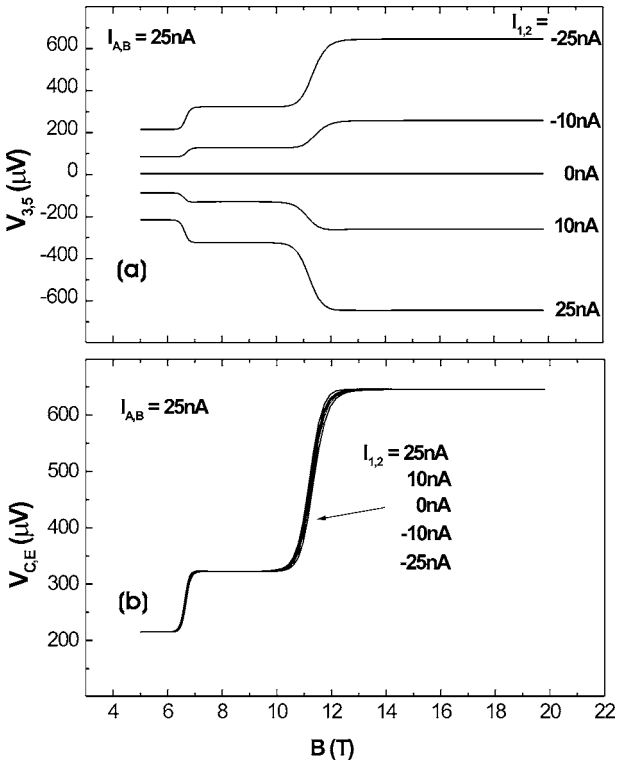

FIG. 5. (a) A network model simulation of the interior anti-Hall bar Hall voltage $V_{3,5}$ at different $I_{1,2}$ and constant exterior current $I_{A,B}=25$ nA. The interior Hall voltage $V_{3,5}$ is proportional to the interior current $I_{1,2}$. (b) Simulation of the exterior (Hall bar) Hall voltage $V_{C,E}$ at different currents $I_{1,2}$ and constant exterior current $I_{A,B}=25$ nA. The exterior Hall voltage $V_{C,E}$ is insensitive to the interior current $I_{1,2}$.

An effective mass of $m^*=0.07$ has been used for calculating the occupation numbers of the LL's and the lateral carrier density profile. The effective g factor has been set to $g^*=7$ in order to achieve full spin splitting. A magnetic field dependent LL broadening was realized with $\Gamma=\Gamma_0 B^{1/2}$ and $\Gamma_0=0.5$ meV.[15]

As indicated in Fig. 3, two currents are injected into the sample. $I_{A,B}$ is applied via the outer boundary and held constant at 25 nA, while $I_{1,2}$ is applied via the inner boundary of the sample and it is incremented between different magnetic field sweeps from $I_{1,2}=-25$ nA to +25 nA. As shown in Fig. 5(a), the Hall voltage $V_{3,5}$ at the inner boundary (anti-Hall bar) is proportional to $I_{1,2}$ while the Hall voltage $V_{C,E}$ at the outer boundary (Hall bar) is insensitive to the current $I_{1,2}$ [see Fig. 5(b)]. The polarity of $V_{C,E}$ for a current $I_{A,B}$ flowing from left to right via the outer boundary is the same as the polarity of $V_{3,5}$ for $I_{1,2}$ flowing in opposite direction via the inner boundary. Remarkably, two different quantized Hall voltages can be observed simultaneously in this configuration, and each depends only on the current injected via the corresponding boundary.

Figure 6 shows the simulation of the longitudinal voltages at the inner and outer boundaries and they are found to be identical and proportional to the sum of the supplied currents. It seems not to matter which current ($I_{1,2}$ or $I_{A,B}$) is fixed and which current ($I_{1,2}$ or $I_{A,B}$) is varied. For example,

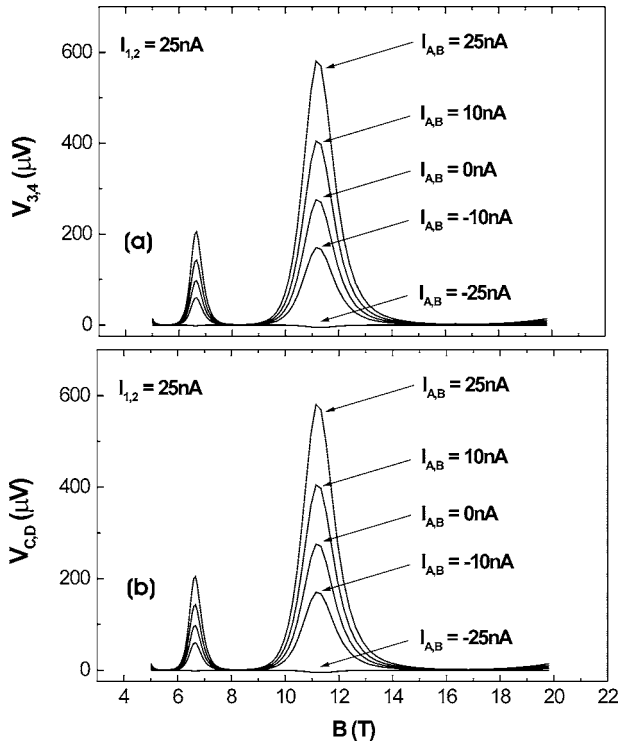

FIG. 6. A network model simulation of (a) the longitudinal voltage $V_{3,4}$ at the anti-Hall bar and (b) the longitudinal voltage $V_{C,D}$ at the Hall bar. Panel (a) and (b) are identical because the longitudinal voltages are insensitive to the boundary of origin of the current, unlike the Hall voltages. Note that the diagonal voltages vanish at current compensation, $I_{A,B}=-I_{1,2}$.

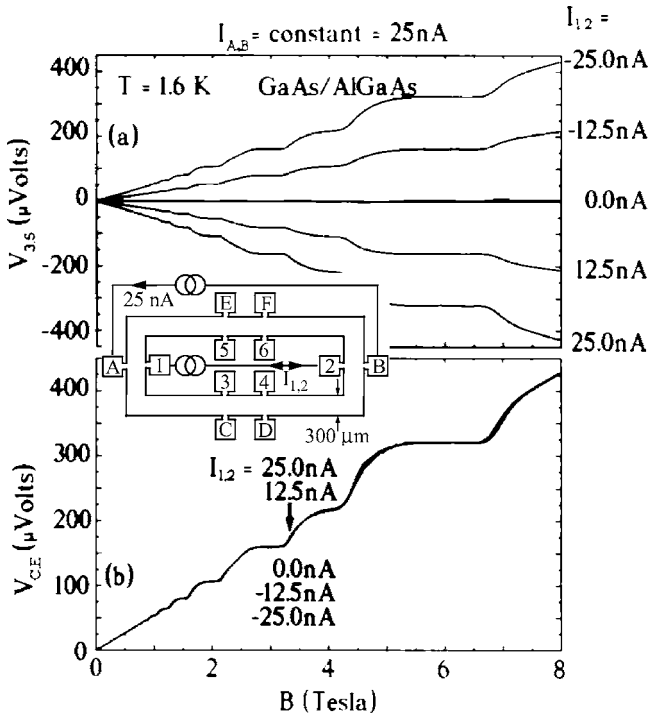

FIG. 7. Experimental data of Mani (Refs. 6–8). Inset: The anti-Hall bar within a Hall bar configuration. The voltage probes and current contacts are labeled as in the simulation of Fig. 5. (a) The interior Hall voltage $V_{3,5}$ with $-25 \leqslant I_{1,2} \leqslant +25$ nA and fixed current $I_{A,B}=25$ nA. (b) The exterior Hall voltage $V_{C,E}$ under the same conditions remains unchanged.

if $I_{1,2}$=const=25 nA and $I_{A,B}$ varies from $-25\ \text{nA} < I_{A,B} < 25$ nA, as in the case of Fig. 6, the voltages $V_{3,4}$ and $V_{C,D}$ increase at the same rate from zero under current compensation—i.e., $I_{A,B}=-I_{1,2}$—to a maximum value at $I_{A,B}=I_{1,2}$, and there is almost no difference between Figs. 6(a) and 6(b).

In experiments, Mani used a GaAs/AlGaAs single heterostructure with a carrier density of $n_0=3\times10^{11}$ cm^{-2} and a mobility $\mu(4.2\ \text{K})=0.3-0.5\times10^6$ cm^2/V s. The layout of the sample is shown in Fig. 1. The experimental Hall effect results are shown in Figs. 7(a) and 7(b), and one can see that the trends seen in the Hall effects are in good agreement with the trends obtained in the simulations (Fig. 5).

So far as the longitudinal voltages are concerned, the simulations (Fig. 6) should be compared with the experimental longitudinal voltage data shown in Fig. 8. Simple inspection suggests that that there is almost no difference between the longitudinal voltage measured at the outer and inner boundaries in experiment, just as in the simulations.

Figure 9 shows the current density distribution in the bulk, which results from the simulation for the case of current compensation ($I_{A,B}=-I_{1,2}$), for a magnetic field or filling factor that exhibits quantized Hall effect in Fig. 5. It is remarkable, that in this case a single current loop is formed (see also Fig. 10), which contains both current sources connected across the bulk, although the system shows quantized Hall plateaus. This feature confirms that a bulk current can go together with quantized Hall effects.

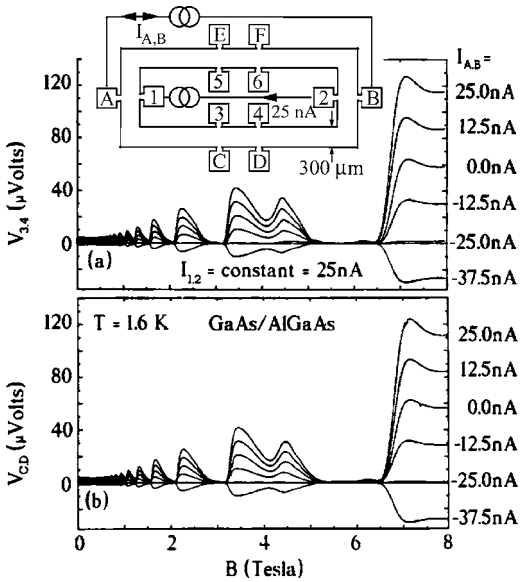

FIG. 8. Experimental data from Refs. 6–8. (a) The longitudinal voltage $V_{3,4}$. (b) The longitudinal voltage $V_{C,D}$. The longitudinal voltages observed on either boundary of the left branch of the sample are identical because the longitudinal voltages are insensitive to the boundary of origin of the current. At current compensation, $I_{A,B}=-I_{1,2}$, the diagonal voltages vanish.

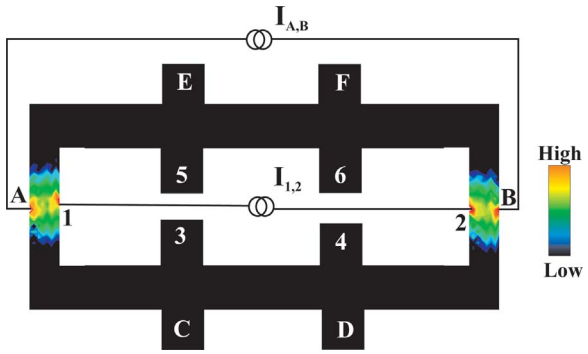

FIG. 9. (Color) The calculated current density distribution, which suggests bulk flow, is illustrated for the case of current compensation ($I_{A,B}=-I_{1,2}$) at a magnetic field of $B=8$ T according to Figs. 5 and 6. The logarithm of the current density is color coded as indicated on the right side. The local currents are obtained from the edge channel picture within each grid period.

IV. DISCUSSION

Laughlin's gauge argument theory is believed to explain the quantized Hall effect that is observed in the experimentally examined Hall bar geometry, although the Hall bar geometry differs topologically from the cylindrical geometry that was examined in his thought experiment.

The experimental investigation of a doubly connected anti-Hall bar within a Hall bar configuration, which appears topologically equivalent to the doubly connected cylinder, has shown that more than one Hall effect can be realized—and observed—at the same time, in a single specimen.[6–8] For the high-magnetic-field regime, Mani gave a possible EC-type interpretation of the two independent Hall effects: If EC's are formed, the absence of backscattering separates the two boundaries and helps to realize a situation corresponding with two disconnected samples, with independent Hall effects. Yet Mani also found that, in the low-magnetic-field regime, the samples showed the same boundary specific Hall effect behavior as in the high-magnetic-field regime, although EC transport should not yet be established. In addition, the low-magnetic-field results for the magnetoresistive

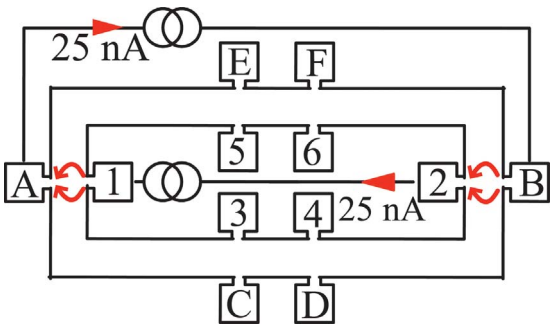

FIG. 10. (Color) A sketch of the current distribution in the anti-Hall bar within a Hall bar geometry in the compensated current configuration, $I_{A,B}=-I_{1,2}$, for which the Hall and diagonal voltages are exhibited in Figs. 5–8, and the calculated current distribution is shown in Fig. 9. The figure shows a bulk current configuration under quantized Hall plateau conditions.

voltage did not show an exclusive dependence on the current injected to a particular edge; it depended, instead, on the total current injected into the sample. From this set of observed features, boundary specificity of the Hall effect in Mani's experiments was attributed to a previously unknown superposition property of Hall's effect.[6–8]

Looking carefully at the plateau transitions, there can be seen a slight broadening in Fig. 5(b) where all Hall traces are plotted on top of each other. Also in the experimental Hall curves in Fig. 7(b) such a slight broadening in the superposition seems to be present. We attribute this effect in the Hall data to a mixing of the longitudinal and the Hall voltage in experiment resulting from Hall voltage contact misalignment and to the discretization of the network in the simulation. Thus, the observed transition broadening seems not to require new physics.

Once again, it appears worth pointing out that on the one hand one obtains two independent Hall voltages (depending only on the current supplied to the corresponding edge) but on the other hand only one longitudinal voltage, which is the same taken either at the outer or inner voltage probes (depending only on the sum of the currents supplied to the outer and inner edge). From this point of view, the bulk of the sample seems to contribute homogeneously, which is in contradiction with the idea that the edge is exclusively responsible for transport.

In this context it is interesting to see how our network model deals with this situation. The simulation data show that we get the proper Hall voltages as well as the correct behavior of the longitudinal voltage. Although the theoretical basis of our network model seems to be the EC picture, it has been shown already, that it is possible to generalize the Buttiker formalism in order to combine edge and dissipative bulk transport.[10] This has led to the introduction of the backscattering function P, which is also used as the basis of the network model. In Ref. 12, we demonstrated that the most likely mechanism for bulk current transport is quantum tunneling between magnetic bound states, which are caused by long-range potential fluctuations in the high-magnetic-field regime. At the same time, we also showed that our network approach is equivalent to a bulk current picture in terms of mixed phases of different quantum Hall liquids. This is demonstrated by Fig. 9, where the simulation results for current compensation in the quantized Hall plateau region clearly indicate the existence of a bulk current, which connects both current sources to a single current loop, which maintains current conservation. Therefore, we believe to have found a suitable network representation, which covers edge and bulk effects in the right way, close to the experimental conditions. As a consequence, most experimental restrictions like the necessity of metallic contacts and edges exist also for our network model. Nevertheless, there is more flexibility for designing different sample structures within the network model than in real experiments. There are further experiments by Mani using gates on the anti-Hall bar within a Hall bar structures,[16,17] which are also accessible by our network model and which we hope to address in a future publicaton. Another topic of our ongoing work is the investigation of the low-magnetic-field regime, where the QHE plateaus are not yet established.

V. SUMMARY AND CONCLUSION

We briefly introduced a network model for magnetotransport in two-dimensional electronic systems and presented simulation results for the so-called "anti-Hall bar within a Hall bar" configuration, which is a doubly connected two-dimensional plate that is driven simultaneously by two independent floating current sources.

In full agreement with Mani's experiments, we have demonstrated that one obtains simultaneous independent Hall voltages at the inner (anti-Hall bar) and outer boundary (Hall bar) of the anti-Hall bar within a Hall bar configuration, with each Hall voltage depending exclusively on the current injected into the corresponding boundary. In contrast, the longitudinal voltages are not boundary specific. They depend on the sum of the injected currents and appear identical at the Hall bar and anti-Hall bar, as demonstrated by experiment and network-model based numerical simulations.

Thus, experimentally observed voltages in the anti-Hall bar with a Hall bar configuration indicate, at the same time, both edgelike and bulklike characteristics, although the current seems not to be restricted to the edge. The network model examined here captures these features by modeling the sample as a network of saddle points, where each saddle point (node) in the bulk is treated in an EC picture. In essence, the model examined here is a generalization of the edge channel picture for the bulk transport regime. The excellent agreement between our simulations and experiments for even such a complex system as the doubly connected two-dimensional electron device opens the possibility of addressing, in detail, further interesting questions related to the nature of the current and voltage distribution in the two-dimensional electron system at high magnetic fields.

[1] *The Quantum Hall Effect*, 2nd ed., R. E. Prange and S. M. Girvin (Springer-Verlag, New York, 1990).
[2] R. B. Laughlin, in *The Quantum Hall Effect*, edited by R. E. Prange and S. M. Girvin (Springer-Verlag, New York, 1987), p. 234.
[3] M. Büttiker, Phys. Rev. B **41**, R7906 (1990).
[4] T. Christen and M. Büttiker, Phys. Rev. B **53**, 2064 (1996).
[5] S. Komiyama, O. Astafiev, and T. Machida, Physica E (Amsterdam) **20**, 43 (2003).
[6] R. G. Mani, J. Phys. Soc. Jpn. **65**, 1751 (1996).
[7] R. G. Mani, Europhys. Lett. **34**, 139 (1996).
[8] R. G. Mani, Europhys. Lett. **36**, 203 (1996).
[9] J. Oswald and A. Homer, Physica E (Amsterdam) **11**, 310 (2001).
[10] J. Oswald, Physica E (Amsterdam) **3**, 30 (1998).
[11] J. Oswald, G. Span, and F. Kuchar, Phys. Rev. B **58**, 15401 (1998).
[12] J. Oswald, cond-mat/0411527 (unpublished).
[13] J. T. Chalker and P. D. Coddington, J. Phys. C **21**, 2665 (1988).
[14] D. B. Chklovskii, B. I. Shklovskii, and L. I. Glazmann, Phys. Rev. B **46**, 4026 (1992).
[15] M. Russ, A. Lorke, D. Reuter, and P. Schafmeister, Physica E (Amsterdam) **22**, 506 (2004).
[16] R. G. Mani and K. von Klitzing, Z. Phys. B: Condens. Matter **92**, 335 (1993); R. G. Mani, Phys. Rev. B **55**, 15838 (1997).
[17] R. G. Mani, Appl. Phys. Lett. **70** 2879 (1997).